ELSEVIER

Chemical Engineering Science 58 (2003) 4911–4919

Chemical Engineering Science

www.elsevier.com/locate/ces

Mathematical modelling of the unsteady-state oxidation of nickel gauze catalysts

Bastien Monnerat, Lioubov Kiwi-Minsker, Albert Renken*

Laboratory of Chemical Reaction Engineering, Swiss Federal Institute of Technology Lausanne (EPFL), CH-1015 Lausanne, Switzerland

Received 17 July 2002; received in revised form 20 November 2002; accepted 22 November 2002

Abstract

The oxidation of nickel gauze catalysts by O_2 was investigated by transient response methods. Qualitative description of the experimental transient responses have shown that the oxidation of metallic nickel proceeds in two stages. The first step is a fast dissociation of gaseous oxygen on the catalytic surface, followed by oxygen diffusion from the surface into the bulk. This slow second step explains the long tailing observed from the experimental transient responses. Furthermore, a rise of temperature was observed during the nickel oxidation. A kinetic model has been developed on the basis of the experimental results in order to provide quantitative information about this reaction. For nickel gauze oxidation, a non-isothermal model combining the subsurface oxygen diffusion with an exponential distribution for the activity of surface sites gave a good agreement with experimental transient data. As a result, the activation energies and the pre-exponential factors of the rate constants as well as the characteristic oxygen diffusion times were determined.

Keywords: Mathematical modelling; Reaction/convection/diffusion problem; Structured catalyst; Oxidation; Nickel; Transient

1. Introduction

Nickel catalysts are widely used in many important industrial processes like hydrogenation of oil, hydrogen production through partial oxidation, steam reforming or autothermal reforming of hydrocarbons. Recently, we reported an attractive method to produce carbon oxide-free hydrogen by catalytic cracking of methane over nickel gauze (Monnerat, Kiwi-Minsker, & Renken, 2001). The catalyst deactivates due to intensive coke deposition. Therefore, the reactor was operated periodically with the cracking followed by the catalyst regeneration by burning off coke in oxidative atmosphere. The integral selectivity for hydrogen was found to depend strongly on the oxidation state of the catalyst after the regeneration period.

During CH_4 passage over a totally reduced Ni catalyst, only hydrogen and unconverted methane was observed, whereas after oxidative regeneration, CO, CO_2 and H_2O were formed. The formation of these products can be explained by the formation nickel oxide and some oxygen adsorbed on the catalyst surface, which interacts with methane. Therefore, the degree of oxidation is a crucial parameter for the CO formation and in consequence the purity of the hydrogen formed. As the degree of oxidation depends on the length and temperature of the regeneration period a quantitative relationship is necessary for the choice of optimal reaction conditions.

The aim of the present study is to provide a quantitative description of Ni oxidation kinetics, which will be integrated into the reaction scheme of H_2 production describing the cycles of catalyst deactivation and regeneration.

The step-response method, which consists of the measurement of the response of a catalytic system on a step-wise change in the concentration of reactants, was chosen for the substantial amount of information that it provides (Kobayashi, 1982; Tamaru, 1983; Renken, 1993; Randall, Doepper, & Renken, 1998).

2. Experimental

The reaction was carried out in a tubular reactor (ID = 9 mm and $L = 230$ mm). Metallic nickel in the form of wire gauze was used as a catalyst. The main advantages of this kind of catalyst are the regular open structure and

* Corresponding author. Tel.: +41-21-693-3181; fax: +41-21-693-3190.
E-mail address: albert.renken@epfl.ch (A. Renken).

0009-2509/$ - see front matter © 2003 Elsevier Ltd. All rights reserved.
doi:10.1016/j.ces.2002.11.006

the flexibility that enables to use them in structured catalytic beds (Monnerat et al., 2001). In order to increase the specific surface area of bulk nickel, a Raney-type outer layer was formed on the metal surface (Wainwright, 1997; Monnerat et al., 2001; Kiwi-Minsker, 2002). Experiments were performed with the modified nickel gauze ($\sim$ 210 mg), placed in the middle part of the reactor in a rolled form (length 20–30 mm) between two inert packings of quartz beads. Residence time distribution measurements have shown that the behaviour corresponds to a plug flow reactor. Details of the experimental set-up are described elsewhere (Monnerat, 2001). Prior to each step of oxygen, the catalyst was reduced during 4 h in a gas flow containing 10 vol% hydrogen in argon at a temperature of 773 K ($Q = 75$ ml (STP)/min, $p_{tot} = 1.5$ bar). Afterwards the reactor was purged with argon and the reaction conditions were adjusted. The reactor effluents were monitored continuously by a mass spectrometer.

3. Results and discussion

3.1. Qualitative interpretations of the transient responses

The oxidation of metal is a complex process depending on a large number of parameters such as the homogeneity of the surface, the metal composition, the morphology and the experimental conditions (temperature, pressure and gas-phase composition).

The kinetics of nickel oxidation were described in several papers: (Labohm, Gijzeman, & Geus, 1983; Leclercq, Pietrzyk, Gengembre, & Leclercq, 1986; Hoang-Van, Kachaya, Teichner, Arnaud, & Dalmon, 1989; Vreeburg, vanKooten, Gijzeman, & Geus, 1992a; Vreeburg, Tongeren, Gijzeman, & Geus, 1992b; Stuckless, Wartnaby, Al-Sarraf, Dixon-Waren, Kovar, & King, 1997; Gellings & Bouwmeester, 2000). Most of these studies were carried out on mono-crystals in ultrahigh vacuum at temperatures under 600 K. The results obtained show that the surface coverage by oxygen species is higher than one indicating a multilayer oxygen adsorption. In contrast to the mentioned studies, the present experiments were carried out under atmospheric pressure and at temperatures higher than 700 K.

Fig. 1 shows the typical response of a reduced Ni catalyst to a step-change of O_2 concentration (molar fraction) from 0 to 0.08 at the reactor inlet. The transient response of O_2 is compared to the response of the reactor to an inert tracer (N_2) with the same inlet concentration of 0.08. It is seen that the initial rate of oxidation is very fast resulting in an almost complete consumption of oxygen and leads to an important temperature increase of the catalyst (up to 50 K) as shown in Fig. 1b.

After approximately 10 s oxygen appears at the reactor outlet indicating a decreasing conversion. Furthermore, the oxygen response is characterised by an important tailing and the inlet concentration of oxygen is reached only after

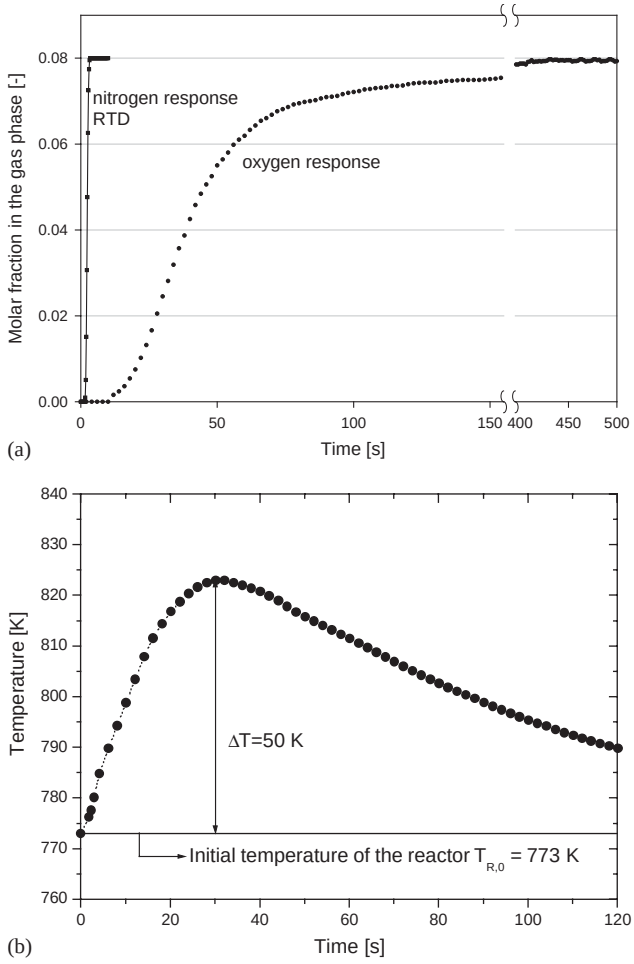

Fig. 1. (a) Typical transient response of oxygen to a concentration step of Ar → 8% O_2/Ar on the totally reduced catalyst. (b) Evolution of temperature measured in the middle of the reactor. Experimental conditions: $y_{O_2,0} = 0.08$, $Q = 75$ N ml/min, T = 773 K, $m_{cat} = 213$ mg, $p_t = 150$ kPa.

10–30 min depending on the reaction temperature. The long transient period can be explained by the slow diffusion of oxygen from the surface into the bulk of the metallic Ni (Vreeburg et al., 1992a, b). For temperatures above 600 K, Vreeburg et al. report that a large amount of oxygen can be dissolved in the nickel crystal and the surface is only partly covered by oxygen in contrast to the results obtained at lower temperatures. The author concludes that at elevated temperatures the reaction proceeds in two consecutive steps: firstly, the oxygen chemisorpts on the surface and dissociates, and then it diffuses into the bulk. In addition (Stuckless et al., 1997) report that the heterogeneity of the surface can lead to an important decrease of the oxidation rate since the adsorption of oxygen decreases with the amount of oxide present at the surface (the oxygen sticking probability diminishes with the oxygen coverage).

3.2. Oxygen capacity of the nickel catalyst

The total amount of oxygen incorporated in the nickel catalyst was estimated from transient oxidation and

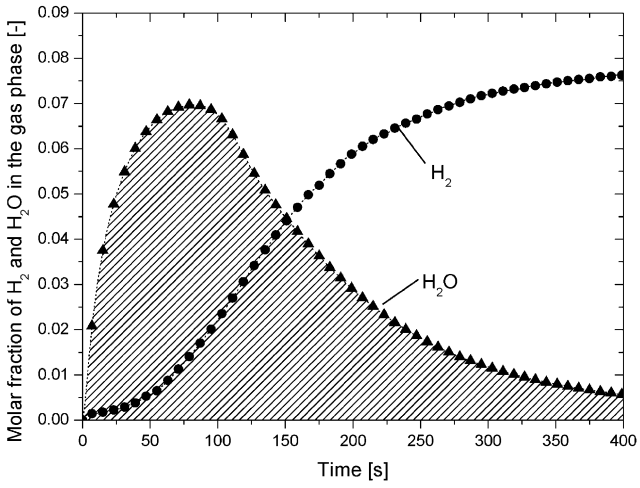

Fig. 2. Typical transient response to a step of H_2 on a partially oxidised catalyst (25% NiO). Experimental conditions: $y_{H_2,0}=0.1$, $Q=75$ N ml/min, $T=773$ K, $m_{cat}=213$ mg, $p_t=150$ kPa.

Table 1
Determination of the oxygen capacity of the catalyst by oxidation of the totally reduced catalyst, $T=773$ K, $Q=75$ N ml/min, $p_t=150$ kPa, $y_{O_2,0}=0.08$

$y_{O_2,0}$, dimensionless	Consumption of O_2, mol/kg$_{cat}$
0.04	1.15
0.06	1.21
0.08	1.23
0.1	1.22

reduction. The oxygen capacity was obtained by integrating the oxygen responses for different concentration steps of O_2 at the reactor inlet (Fig. 1a):

$$n_{O_2}=\frac{F_{tot}}{m_{cat}}\int_0^{50\ min}(y_{O_2,0}-y_{O_2(t)})\,dt. \quad (1)$$

Similarly, as shown in Fig. 2, the total amount of H_2O produced by reducing the oxidized nickel catalyst was determined by integrating the hydrogen responses and the water formation. The amount of H_2 converted is given by

$$n_{H_2}=\frac{F_{tot}}{m_{cat}}\int_0^{50\ min}(y_{H_2,0}-y_{H_2(t)})\,dt. \quad (2)$$

The totally produced quantity of water during the reduction of the nickel gauze is given by

$$n_{H_2O}=\frac{F_{tot}}{m_{cat}}\int_0^{50\ min}y_{H_2O(t)}\,dt. \quad (3)$$

The results obtained for different inlet concentrations of oxygen and hydrogen are presented in Tables 1 and 2 . The results are well reproducible and confirm the reversibility of the reduction/oxidation process. The maximum capacity of the nickel catalyst is estimated to be 1.2 mol(O_2) kg$_{cat}^{-1}$.

Table 2
Determination of the oxygen capacity of the catalyst by reduction of the partially oxidised catalyst (25% NiO), $T=773$ K, $Q=75$ N ml/min, $p_t=150$ kPa and $y_{H_2,0}=0.1$

$y_{H_2,0}$, dimensionless	Consumption of H_2, mol/kg$_{cat}$	Production of H_2O, mol/kg$_{cat}$
0.05	2.32	2.35
0.08	2.36	2.41
0.1	2.41	2.43

Taking into account the subsurface diffusion the value of 2.4 mol(O) kg$_{cat}^{-1}$ is in the range of those observed on monocrystals at lower temperatures (100–500 K). Typical values reported for oxygen coverage at low temperatures vary in a range from 1 to 7 monolayer (ML) (Labohm et al., 1983; Leclercq et al., 1986; Hoang-Van et al., 1989; Vreeburg et al., 1992a, b; Stuckless et al., 1997; Gellings & Bouwmeester, 2000). 1 ML (monolayer) corresponds to approximately 1.9×10^{15} atoms/cm^2. For the nickel gauze used in this work with a specific surface of 25 m^2/g, the corresponding oxygen capacity is in 0.8 mol(O) kg^{-1}).

3.3. Modelling

To describe the dynamic experiments, a kinetic model was developed based on the following assumptions: oxygen is dissociatively chemisorbed on the surface (Eq. (4)) and diffuses slowly in a consecutive step into a subsurface layer (Eq. (5))

$$O_2+2Ni\rightarrow 2O\text{–}(Ni), \quad (4)$$

$$O\text{–}(Ni)\rightarrow (NiO). \quad (5)$$

The oxidation rate (r_{ox}) (Eq. (6)) is assumed to be first order towards oxygen and second order towards reduced sites ($\theta_{v,s}$) (Labohm et al., 1983):

$$r_{ox}=k'_{ox}c_{O_2}\,\theta_{v,s}^2=k_{ox}\,c_{O_2}(1-\theta_{O,s})^2, \quad (6)$$

where k'_{ox} is the rate constant, $\theta_{v,s}$, $\theta_{O,s}$ the fraction of reduced and oxidised sites, respectively, and c_{O_2} the concentration of oxygen in the gas-phase.

As mentioned above, the surface heterogeneity can lead to a significant decrease of the oxidation rate since the chemisorption depends strongly on the oxygen coverage. Therefore, in agreement with the Brunauer, Love and Keenan equation for the adsorption rate constant on non-ideal surface (Carberry, 1976), activity sites distribution is introduced, assuming an exponential decrease of the rate constant with the occupied O–(Ni) sites:

$$k_{ox}=k'_{ox}\exp(-g\theta_{O,s}). \quad (7)$$

This equation can be derived from the assumption that the activation energy is a linear function of $\theta_{O,s}$, as

defined by Eq. (8). The physical bases for this assumption can be surface heterogeneity, lateral interaction between adsorbed-species or a combination of them (Carberry, 1976; Do, 1998).

$$E^*_{a,\mathrm{ox}} = E_{a,\mathrm{ox}} + \gamma\theta_{\mathrm{O},s}. \tag{8}$$

The Arrhenius equation can hence be written, (Eq. (9)). This equation expresses that the surface reaction rate diminishes at high oxygen coverage.

$$k_{\mathrm{ox}} = A\exp\left(-\frac{E_{a,\mathrm{ox}} + \gamma\theta_{\mathrm{O},s}}{\mathrm{RT}}\right) = A\exp\left(-\frac{E_{a,\mathrm{ox}}}{\mathrm{RT}}\right)\exp(-g\theta_{\mathrm{O},s}) \quad \text{with } g = \frac{\gamma}{\mathrm{RT}}. \tag{9}$$

4. Mass balance equations

As shown in Fig. 1a, at the beginning of the dynamic experiment, the oxidation reaction is very fast and the conversion of oxygen reaches high values up to 100% in the first seconds. This gives rise to a significant concentration gradient of oxygen in the axial direction of the fixed bed. Therefore, the reactor cannot be taken as differential (gradientless), but has to be treated as an integral reactor (Fig. 3). Mass transfer limitations cannot be excluded within the first 10–20 s after the switch to oxygen. But, as the conversion of O_2 is nearly complete within this period, an estimation of the influence of mass transfer is hardly possible. After the short initial period oxygen accumulates on the surface leading to a decrease of the adsorption rate (Eq. (7)) and the influence of mass transfer becomes negligible.

4.1. Mass balance for gas-phase species

The mass balance equation for oxygen in the gas phase in a heterogeneous catalytic reactor with plug flow behaviour is given by Eq. (10). The residence time distribution is reported in Figure 1a confirming plug flow behaviour of the reactor. Therefore, axial dispersion is neglected in this model.

$$\frac{\partial c_{\mathrm{O}_2}}{\partial t} = -u_g\frac{\partial c_{\mathrm{O}_2}}{\partial x} + \rho_{\mathrm{cat}}\frac{(1-\varepsilon)}{\varepsilon}R_{\mathrm{O}_2}, \tag{10}$$

where u_g is the gas velocity, ρ_{cat} the catalyst bulk density, ε the bed porosity and R_{O_2} the rate of oxygen consumption. The gas velocity is given by

$$u_g = \frac{Q}{\varepsilon S} = \frac{4Q}{\varepsilon\pi d_R^2} = \frac{4T_R}{T_0}\frac{p_0}{p}\frac{Q_0}{\varepsilon\pi d_R^2}. \tag{11}$$

The rate of oxygen consumption, R_{O_2}, is given by

$$R_{\mathrm{O}_2} = -r_{\mathrm{ox}}. \tag{12}$$

The concentration of oxygen in the gas-phase, c_{O_2}, is converted to the molar fraction y_{O_2} via the ideal gas law.

4.2. Initial and boundary conditions for the gas-phase species

For an oxygen concentration step from 0 to $y_{\mathrm{O}_2,0}$ at $t = 0$, the initial condition is

$$c_{\mathrm{O}_2}(x, 0) = 0. \tag{13}$$

The boundary condition at the reactor inlet ($x = 0$) is given by

$$c_{\mathrm{O}_2}(0, t) = \frac{p_R}{\mathrm{RT}_R}\, y_{\mathrm{O}_2,0}(t). \tag{14}$$

By solving Eq. (10), the concentration gradient of the gas-phase oxygen in the axial direction of the reactor (x) can be obtained. However, the rate of oxygen consumption,

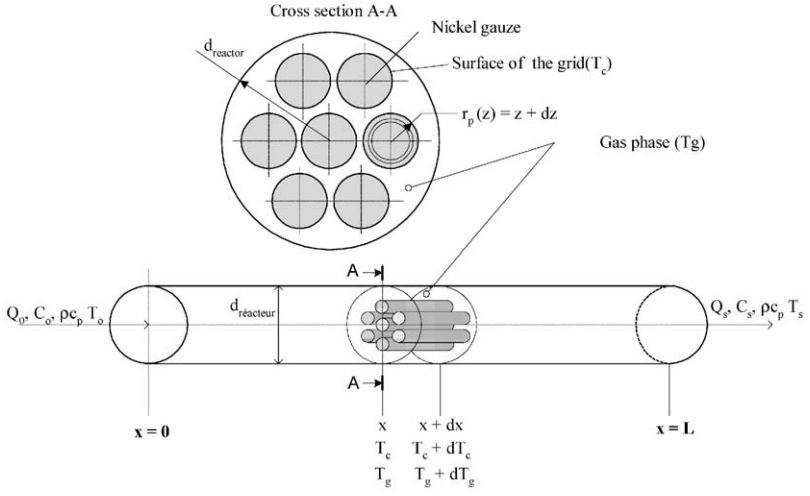

Fig. 3. Schematic presentation of the reactor used for the mathematical modelling.

R_{O_2}, is a function of the oxygen coverage $\theta_{O,s}$ (Eq. (6)). Eq. (10), therefore, has to be solved simultaneously with the mass balance equation for $\theta_{O,s}$.

4.3. Mass balance for oxygen surface species and subsurface oxygen diffusion

Subsurface oxygen diffusion is suggested to explain the long tailing observed in the oxygen responses. Thus, an additional parameter has to be introduced: the distance from the nickel surface into the bulk (z), where diffusion takes place. The oxidation of nickel at the surface ($z = 1$) produces surface oxygen species which diffuse into the subsurface oxygen vacancies, giving rise to a concentration profile of oxidised species θ_O as a function of z. The degree of oxidation of the nickel catalyst is, therefore, a function of x, z and time.

The dimensionless mass balance equation for the degree of oxidation of the nickel gauze at the surface ($z=1$) is given by Eq. (15) expressed in cylindrical coordinates. Eq. (15) indicates that the accumulation of oxygen atoms at the catalyst surface is equal to the net rate at which oxygen atoms diffuse into the metal lattice and the rate at which oxygen atoms are formed by dissociative adsorption.

$$\frac{\partial\theta_O}{\partial t}(x,z=1,t) = -\frac{1}{t_d}\left(\frac{\partial\theta_O}{\partial z}\right)_{z=1} + \frac{R_{\theta_O}}{N_{tot}} \quad \text{with } R_{\theta_O} = -2\,r_{ox}, \tag{15}$$

where t_d is the characteristic diffusion time of oxygen into the nickel bulk. It is given by

$$t_d = \frac{\delta^2}{D} \quad \text{with } \delta = r_p, \tag{16}$$

where D is the diffusion coefficient and δ the thickness of the nickel layer defined by the radius of the nickel gauze r_p.

In the bulk of the nickel catalyst ($z < 1$), only the transport of oxygen by diffusion is assumed. Moreover, no chemical reaction occurs in the bulk of nickel. Consequently, the dimensionless mass balance equation for the bulk ($z < 1$) is given by

$$\frac{\partial\theta_O}{\partial t}(x,z<1,t) = \frac{1}{t_d}\left(\frac{\partial^2\theta_O}{\partial z^2} + \frac{1}{z}\frac{\partial\theta_O}{\partial z}\right). \tag{17}$$

4.4. Initial and boundary conditions for the solid phase

For a totally reduced catalyst, the initial condition for the two-dimensional partial differential Eqs. (15) and (17) is

$$\theta_v(x,z,0) = 1 \quad \text{and} \quad \theta_O(x,z,0) = 0. \tag{18}$$

Due to the symmetry of the cylinder, the boundary condition at the centre of the gauze wires ($z = 0$) is

$$\frac{\partial\theta_O}{\partial z}(x,0,t) = 0. \tag{19}$$

4.5. Energy balance

As shown in Fig. 1b, the oxidation is accompanied by an initial rise of temperature. The temporal temperature variations can significantly affect the transient responses of oxygen.

The long tailing observed in Fig. 1b can be explained by the inertia of the system. Therefore, the energy balance for the gas and the solid phase have to be included in the reactor simulation. The energy balance is developed using the following assumptions:

- No heat diffusion in the gas phase.
- No heat transfer by radiation.
- Adiabatic reactor behaviour.
- Heat production is due to catalytic surface reaction.

The influence of temperature on the physical and thermodynamical properties of solids and gases (viscosity, density, conductivity, heat capacity and reaction enthalpy) was taken into account by using polynomial approximations given by Daubert and Danner (1989). The density of the solid was assumed to be independent of the oxidation state of the catalyst.

4.6. Energy balance for the gas phase

The energy balance for the gas phase considers convection along the axial direction and the heat transfer between the solid and the gas. It is given by

$$\frac{\partial T_g}{\partial t} = -u_g\frac{\partial T_g}{\partial x} + \frac{1}{\varepsilon}\left(\frac{A}{V}\right)\frac{h_{th}}{\rho_g c_{p_g}}(T_c - T_g), \tag{20}$$

where h_{th} is the external heat transfer coefficient and the (A/V) ratio represents the geometric surface of the cylinder (A) to the volume of the gauze (V). The other variables and parameters are defined in the nomenclature section.

4.7. Energy balance for the solid

The energy balance for the solid phase takes into account the heat transport inside the catalyst by axial conduction, the heat transfer from the solid to the gas and the heat production due to surface oxidation of the gauze. Since there is no convective flux in the solid, the energy balance for the solid is given by

$$\frac{\partial T_c}{\partial t} = \frac{\lambda_c}{\rho_c c_{p_c}}\frac{\partial^2 T_c}{\partial x^2} + \frac{1}{(1-\varepsilon)}\left(\frac{A}{V}\right)\frac{h_{th}}{\rho_c c_{p_c}}(T_g - T_c) + \frac{(1-\varepsilon)}{\varepsilon}\frac{(-\Delta H_R)(-R_{\theta_O})}{c_{p_c}}. \tag{21}$$

4.8. Initial and boundary conditions of the energy balance

The initial conditions are given by

$$T_g(0,x) = T_c(0,x) = T_o. \tag{22}$$

Table 3
Physical properties of the reactor system

Physical properties	Values
ρ_g, kg/m^3	1.5
ρ_c, kg/m^3	5×10^3
μ_g, Pa s	3×10^{-5}
Cp_g, J/kg K	1.62×10^3
Cp_c, J/kg K	4.6×10^2
λ_g, W/m K	1.6×10^{-2}
λ_c, W/m K	1×10^2 (Nickel)
ε, dimensionless	8×10^{-1}–9×10^{-1}
r_p, m	4×10^{-5}
$a = A/V$, m^2/m^3	5×10^4
$-\Delta H_R$, J/mol	4.8×10^5

The boundary conditions are given by

$$T_g(t,0) = T_{\text{in}}, \tag{23}$$

$$\left(\frac{\partial T_c}{\partial x}\right)_{x=0} = \left(\frac{\partial T_c}{\partial x}\right)_{x=L} = 0 \quad \forall t. \tag{24}$$

4.9. Determination of gas-solid heat transfer coefficient

The structured gauze catalyst consists of multiple crossed cylinders. For similar geometries, Churchill and Bernstein proposed an empirical correlations to estimate the gas–solid heat transfer coefficient (Churchill & Bernstein, 1977; deSmet, deCroon, Berger, Marin, & Schouten, 1999)

$$Nu = \frac{h_{th} d_p}{\lambda_g} = Nu_0 + \frac{\gamma_1 Re^{1/2} Pr^{1/3}}{[1 + (0.4/Pr)^{2/3}]^{1/4}} \times \left[1 + \left(\frac{Re}{282\,000}\right)^{5/8}\right]^{4/5} \quad (Re\,Pr) > 0.2, \tag{25}$$

with $Nu_0 = 0.3$, $\gamma_1 = 0.6$ (Churchill & Bernstein, 1977).

The physical properties of both gas and solid are summarised in Table 3.

The system of partial differential Equations (10), (15), (17), (20) and (21) was solved using the finite difference approximation method, using 10 nodes in the x direction and 40 nodes in the z direction. In order to obtain stable solutions, centred differences were used for the approximation of parabolic terms (conduction and diffusion) and backward differences for hyperbolic terms (convection) (Ramirez, 1989; Simusolv, 1990; Constantinides & Mostoufi, 1999). Numerical integration was performed using a variable step algorithm (Simusolv, 1990). Optimisation of parameters was performed by fitting the calculated molar fraction of oxygen and both temperatures of the gas and solid to their experimental values, using the Nedler–Mead algorithm and the likelihood function as objective function (Ramirez, 1989; Constantinides & Mostoufi, 1999).

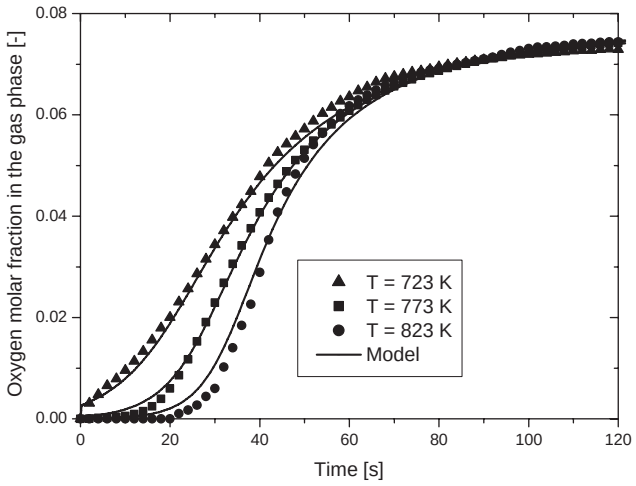

Fig. 4. Typical transient response of oxygen in the reactor outlet on a concentration step of Ar → 8% O_2/Ar over totally reduced catalyst. Simulated and experimental data for different initial reactor temperatures. Experimental conditions: $y_{O_2,0} = 0.08$, $Q = 75$ N ml/min, $m_{cat} = 213$ mg, $p_t = 150$ kPa.

4.10. Reactor simulation

Calculated response curves are compared to experimental results and are presented in Fig. 4 for different initial reactor temperatures. As can be seen, a good prediction of oxygen concentration at the reactor outlet as function of time is obtained in the temperature range from 723 to 823 K.

The temperature dependency of the rate constant k_{ox} and the inverse characteristic time of diffusion, $1/t_d$, is described by the Arrhenius law. The parameter g (Eq. (9)) depends only slightly on the temperature and was kept constant in the studied temperature range. The estimated parameter of the kinetic model are summarised in Table 4.

The simulated spatio-temporal behaviour of the degree of oxidation of nickel catalyst is presented in Fig. 5. In this figure the calculated θ_O profile in the bulk of nickel in the middle of the fixed bed ($x = 0.5$) is given for different reaction times. The degree of oxidation increases drastically at the beginning of the transient due to the heat production generated by the surface oxidation. After that the oxidation rate decreases due to the increase of the surface oxygen coverage.

The rate of the surface oxidation slows down with increasing degree of oxidation. After about 200 s the maximum degree of oxidation at the surface is attained and the rate of oxygen consumption is controlled only by subsurface diffusion. A final degree of oxidation of 88% is reached after 50 min for the experimental conditions given in Fig. 5. This result is in agreement with the observations of Labohm et al. (1983), Vreeburg et al. (1992a, b), and Stuckless et al. (1997) at similar temperatures on monocrystals.

The activation energy of diffusion ($E_{diff} = 54$ kJ/mol) is relatively close to values reported by Randall et al. (1998) (60 kJ/mol) and Castel and Surman (1969) (71 kJ/mol)

Table 4
Optimised model parameters

$E_{a_{ox}}$, kJ/mol	E_{diff}, kJ/mol	$k_{ox,0}$, m^3/kg_{cat} s	$1/td_o$, 1/s	g, dimensionless
69 ± 4	54 ± 6	$3.9 \times 10^3 \pm 2 \times 10^2$	1.3 ± 0.2	4.3 ± 0.2

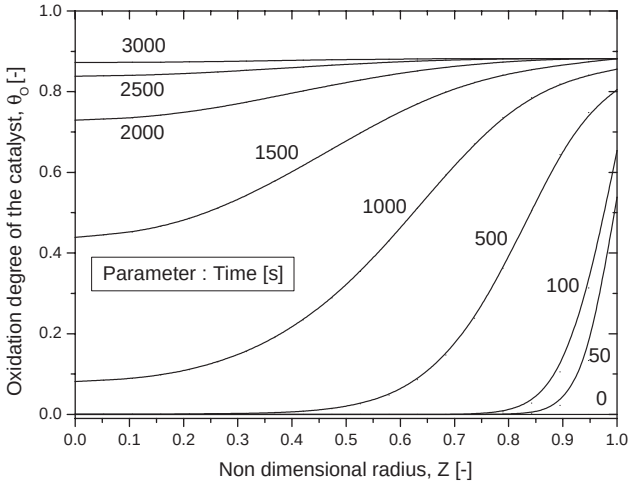

Fig. 5. Calculated spatio-temporal behaviour of the degree of oxidation, θ_O, for an oxygen concentration step on a totally reduced catalyst. Experimental conditions: $y_{O_2,0} = 0.08$, $Q = 75$ N ml/min, $T = 773$ K, $m_{cat} = 213$ mg, $p_t = 150$ kPa.

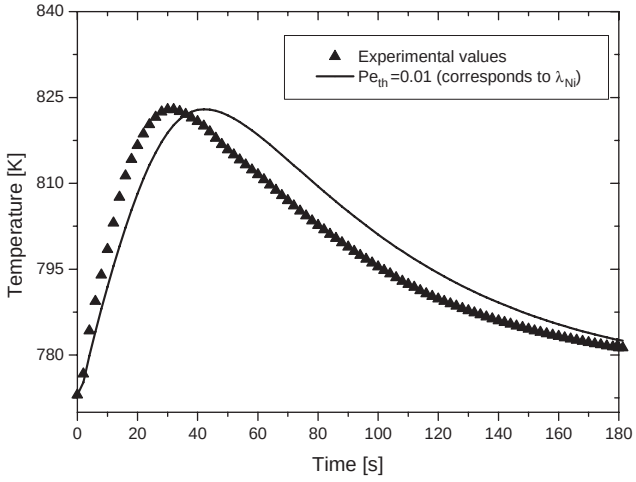

Fig. 6. Simulated and experimental temperature profiles for different initial reactor temperatures. Experimental conditions: $y_{O_2,0} = 0.08$, $Q = 75$ N ml/min, $m_{cat} = 213$ mg, p_t=150 kPa, $Pe_{th} = 0.01$.

for activated diffusion in Fe_2O_3. Furthermore, Al'kaeva, Andrushkevich, Ovsitser, and Sokolovskii (1995) reports a value of 68 kJ/mol for the activation energy for diffusion in a alumina supported catalyst loaded with different metals (Mo, Bi, Fe, Co, Ni, K and Si).

Measured and predicted temperatures under transient conditions are also in good agreement as shown in Fig. 6. Due to the high thermal conductivity of the nickel catalyst (Table 3) and the corresponding small thermal Péclet number of $Pe = 0.01$ (Eq. (26)), axial and radial temperature profiles in the reactor can be neglected

$$Pe = \frac{u_g L_{bed} \rho_g c_{p_g}}{\lambda_c}. \quad (26)$$

Finally, the developed model allows to predict the transient behaviour of the reactor for different inlet concentration of oxygen as shown in Fig. 7.

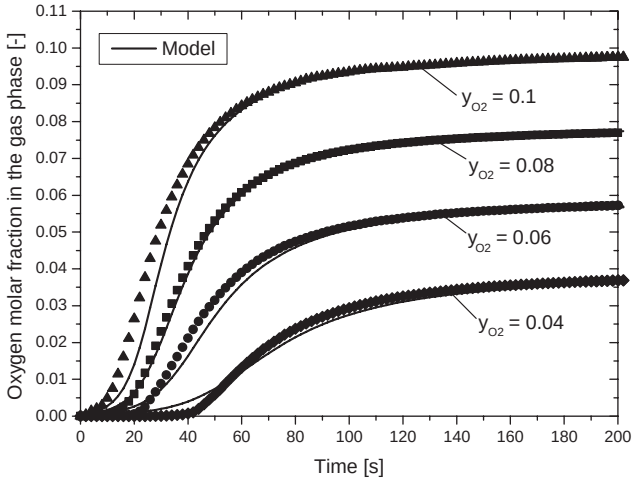

Fig. 7. Predicted and experimental transient responses of oxygen in the reactor outlet on concentration step-changes in the inlet over a totally reduced catalyst at different oxygen molar fractions. Experimental conditions: $Q = 75$ N ml/min, $T = 773$ K, $m_{cat} = 213$ mg, $p_t = 150$ kPa.

5. Conclusions

The oxidation of nickel by O_2 was investigated by transient responses method in order to clarify the redox mechanism. Nickel oxidation/reduction takes place during the production of hydrogen by decomposition of CH_4 in the periodically operated reactor. Non-isothermal model combining the subsurface oxygen diffusion with an exponential activity distribution for the surface sites provided a good description of the transients of nickel oxidation. As a result, the activation energies and the pre-exponential factors of the rate constants as well as the characteristic oxygen diffusion times were determined.

Notation

A	geometric area of the cylinder gauze, m^2
c_p	specific heat, kJ/kg K
c_{O_2}	gas-phase concentration of O_2, mol/m^3
$c_{()}$	oxygen vacancy concentration in the catalyst, mol/kg_{cat}
$c_{(O)}$	bulk oxygen concentration in the catalyst, mol/kg_{cat}
D	diffusion coefficient of oxygen in iron oxide, m^2/s
E_i	activation energy for process i, kJ/mol
g	exponential activity distribution parameter, dimensionless
h_{th}	gas–solid heat transfer coefficient, W/m^2 K
ΔH_R^0	enthalpy of reaction, kJ/mol
k_{ox}	rate constant for oxidation reaction , m^3/kg_{cat} s
k_{i0}	pre-exponential factor, various units, m^3/kg_{cat} s
L	Length, m
m_{cat}	amount of catalyst, kg
n_i	number of moles of species i, mol/kg_{cat}
N_{tot}	total concentration of sites
NTP	normal conditions of temperature and pressure (0°C, 1.013×10^5 Pa)
Nu	Nusselt number, dimensionless
(Ni)	lattice oxygen vacancy
(NiO)	lattice oxygen
p	pressure in the reactor, kPa
Pr	Prandlt number, dimensionless
Q	total volumetric flow rate, ml (NTP)/min
r_{ox}	rate of oxygen chemisorption step mol/kg_{cat} s
r_p	radius of the gauze, m
R	gas constant, kJ/mol K
Re	Reynolds number, dimensionless
R_{O_2}	CO_2 rate of formation, mol/kg_{cat} s
t	time, s
t_d	characteristic diffusion time, s
t_{d0}	characteristic diffusion time at infinite temperature, s
T	temperature, K
V	volume of the cylinder gauze, m^3
x	distance from the reactor inlet, m
X	$(=x/L)$ distance from the reactor inlet, dimensionless
y_{H_2}	hydrogen molar fraction, dimensionless
y_{H_2O}	water molar fraction, dimensionless
$y_{H_2,0}$	hydrogen molar fraction in feed, dimensionless
y_{O_2}	oxygen molar fraction, dimensionless
$y_{O_2,0}$	oxygen molar fraction in feed, dimensionless
z	distance from the centre of the cylindrical-geometry nickel gauze, m
Z	$(=z/\delta)$ distance from the centre of the cylindrical-geometry iron oxide crystallite, dimensionless

Greek letters

γ	exponential activity parameter, kJ/mol
γ_1	empirical parameters for Eq. (25)
δ	thickness of the iron oxide layer, m
ε	void fraction of catalyst, dimensionless
θ_O	bulk oxygen coverage, dimensionless
λ	heat conductivity, W/m K
ρ	density, kg/m^3

Subscripts

0	inlet
bed	catalytic bed
c	index for the catalyst (solid)
d	subscript for subsurface oxygen diffusion process
g	index for the gas
in	reactor inlet
R	index for the reactor
s	index for the surface
v	free sites (reduced nickel)

Acknowledgements

The financial support from the Swiss National Science foundation is gratefully acknowledged.

References

Al'kaeva, E. M., Andrushkevich, T. V., Ovsitser, O. Y., & Sokolovskii, V. D. (1995). Influence of bulk oxygen diffusion on the kinetics of partial oxidation over molybdenum-containing catalysts. *Catalysis Today*, *24*, 357–359.

Carberry, J. J. (1976). *Chemical and catalytic reaction engineering* (pp. 379–382). New York: McGraw-Hill.

Castel, J. E., & Surman, P. L. (1969). The self-diffusion of oxygen in magnetite. The effect of anion vacancy and cation distribution. *Journal of Chemical Physics*, *73*, 632–641.

Churchill, S. W., & Bernstein, M. (1977). A correlating equation for forced convection from gases and liquids to a circular cylinder in crossflow. *Journal of Heat Transfer*, *99*, 300–306.

Constantinides, A., & Mostoufi, N. (1999). Numerical methods for chemical engineers with MatLab applications. *Prentice Hall International serie in the physical and chemical engineering sciences*. New Jersey: Prentice-Hall PTR.

Daubert, T. E., & Danner, R. P. (1989). *Physical and thermodynamics properties of pure chemicals: Data compilation*. New York: Hemisphere Publishing Corp.

deSmet, C. R. H., deCroon, M. H. J. M., Berger, R. J., Marin, G. B., & Schouten, J. C. (1999). An experimental reactor to study the intrinsic kinetics of catalytic partial oxidation of methane in the presence of heat-transport limitations. *Application of Catalysis A: General*, *187*, 33–48.

Do, D. D. (1998). *Absorption analysis: Equilibria and kinetics*. London: Imperial College Press.

Gellings, P. J., & Bouwmeester, H. J. M. (2000). Solid state aspects of oxidation catalysis. *Catalysis Today*, *58*, 1–53.

Hoang-Van, C., Kachaya, Y., Teichner, S. J., Arnaud, Y., & Dalmon, J. A. (1989). Characterization of nickel catalysts by chemisorption

techniques, X-ray diffraction and magnetic measurements: Effect of support, precursor and hydrogen pretreatment. *Application of Catalysis A: General*, *46*, 281–296.

Kiwi-Minsker, L. (2002). Novel structured materials for structured catalytic reactors. *Chimia*, *56*, 143–147.

Kobayashi, M. (1982). Characterization of transient response curves in heterogeneous catalysis: 1-Classification of the curves. *Chemical Engineering Science*, *37*, 393–401.

Labohm, F., Gijzeman, O. L. J., & Geus, J. W. (1983). The interaction of oxygen with Ni(111) and the reduction of the surface oxide by carbon monoxide and by hydrogen. *Surface Sciences*, *135*, 409–427.

Leclercq, G., Pietrzyk, S., Gengembre, L., & Leclercq, L. (1986). Bimetallic Ni-Rh catalysts: 1-Surface composition and chemisorption properties. *Application of Catalysis A: General*, *27*, 299–312.

Monnerat, B. (2001). Production d'hydrogène en regime périodique à partir d'hydrocarbures sur des catalyseurs structurés. EPFL Thèse 2424.

Monnerat, B., Kiwi-Minsker, L., & Renken, A. (2001). Hydrogen production by catalytic cracking of methane over nickel gauze under periodic operation. *Chemical Engineering Sciences*, *56*, 633–639.

Ramirez, W. F. (1989). *Computational methods for process simulation. Butterworths series in chemical engineering*. London: Butterworth Publishers.

Randall, H., Doepper, R., & Renken, A. (1998). Reduction of nitrogen oxides by carbon monoxide over an iron oxide catalyst under dynamic conditions. *Application of Catalysis*, *B17*, 357–359.

Renken, A. (1993). Transient operation for the purpose of modeling heterogeneous catalytic reactions. *International Chemical Engineering*, *33*, 71.

Simusolv, G. (1990). Modeling and simulation software. *Reference guide*. Midland, USA: Dow Chemical Compagny.

Stuckless, J. T., Wartnaby, C. E., Al-Sarraf, N., Dixon-Waren, S. J. B., Kovar, M., & King, D. A. (1997). Oxygen chemisorption and oxide film growth on Ni {100}, {110} and {111}: Sticking probabilities and microcalorimetric adsorption heats. *Journal of Chemical Physics*, *106*, 2012–2030.

Tamaru, K. (1983). Dynamic relaxation methods in catalysis. *Catalysis*: *Science and technology*, Vol. 9 (pp. 89–129). Berlin: Springler-Verlag.

Vreeburg, R. J., vanKooten, W. E. J., Gijzeman, O. L. J., & Geus, J. W. (1992a). The reduction of oxidized Ni(111)-Fe surfaces by hydrogen. *Surface Science*, *262*, 287–293.

Vreeburg, R. J., Tongeren, P. K. V., Gijzeman, O. L. J., & Geus, J. W. (1992b). A comparison between the reduction kinetics of oxidized Ni(111) and Ni(100) surfaces by hydrogen and deuterium. *Surface Science*, *272*, 294–298.

Wainwright, M. S. (1997). *Handbook of heterogeneous catalysis*, Vol. 1 (pp. 64–72). In G. Ertl, H. Knötzinger, & J. Weitkamp (Eds.), New York: Wiley.